Morphology-tuned wurtzite-type ZnS nanobelts

ZHONGWU WANG[1]*, LUKE L. DAEMEN[1], YUSHENG ZHAO[1], C. S. ZHA[2], ROBERT T. DOWNS[3], XUDONG WANG[4], ZHONG LIN WANG[4] AND RUSSELL J. HEMLEY[5]

[1] Los Alamos National Laboratory, Los Alamos, New Mexico 87545, USA
[2] CHESS, Wilson Laboratory, Cornell University, Ithaca, New York 14853, USA
[3] Department of Geosciences, University of Arizona, Tucson, Arizona 85721, USA
[4] School of Materials and Engineering, Georgia Institute of Technology, Atlanta, Georgia 30332, USA
[5] Geophysical Laboratory, Carnegie Institution of Washington, Washington DC 20015, USA
*e-mail: z_wang@lanl.gov

Nanometre-sized inorganic dots, wires and belts have a wide range of electrical and optical properties, and variable mechanical stability and phase-transition mechanisms that show a sensitive dependency on size, shape and structure. The optical properties of the semiconductor ZnS in wurtzite structures are considerably enhanced, but the lack of structural stability limits technological applications. Here, we demonstrate that morphology-tuned wurtzite ZnS nanobelts show a particular low-energy surface structure dominated by the $\pm\{2\bar{1}0\}$ surface facets. Experiments and calculations show that the morphology of ZnS nanobelts leads to a very high mechanical stability to ~6.8 GPa, and also results in an explosive mechanism for the wurtzite-to-sphalerite phase transformation together with in situ fracture of the nanobelts. ZnS wurtzite nanobelts provide a model that is useful not only for understanding the morphology-tuned stability and transformation mechanism, but also for improving synthesis of metastable nanobelts with quantum effects for electronic and optical devices.

ZnS has been extensively investigated as an important wide-band-gap semiconductor (3.6 eV). It is one of the oldest and probably one of the most important materials in the electronics industry with a wide range of applications including light-emitting diodes and efficient phosphors in flat-panel displays[1]. An assortment of luminescent properties excited by ultraviolet, X-ray, cathode ray or electrical currents have been observed by doping ZnS with various metals[2]. Excellent light transmission with a high index of refraction (2.27 at 1 μm) also makes ZnS useful in photonic crystal devices that operate in the region from visible to near-infrared[3].

At ambient conditions, ZnS shows two structural polymorphs: hexagonal wurtzite and cubic sphalerite[4]. Surprisingly, wurtzite ZnS is much more desirable for its optical properties than the sphalerite phase[5]. For instance, phosphors of ZnS are synthesized in the wurtzite phase to optimize luminescence at a temperature near 1,000 °C (ref. 5), because bulk wurtzite crystallizes at temperatures above 1,035 °C. However, the quenched wurtzite easily transforms to the sphalerite form at ambient conditions[5,6]. Decreasing the particle size lowers the temperature boundary and nanosized wurtzite can be synthesized at temperatures 400 °C lower than the bulk[7]. Thus, it seems that it may be possible to synthesize the ZnS wurtzite phase and keep it stable at room conditions by adjusting the surface energy through particle-size tuning. Synthesis of nanoscale semiconductors demonstrates that the quantum-confinement effect can markedly vary optical and electrical properties, mostly resulting in their improvement relative to those of their bulk counterparts[8,9]. These enhanced properties have also been observed in three-dimensional wurtzite ZnS nanocrystals obtained in a variety of ways[10], but the structural instability remains analogous to its bulk counterpart[5].

Here, we report the experimental discovery of ultrastable one-dimensional wurtzite ZnS nanobelts, the morphology-tuned explosive transformation mechanism to the sphalerite form, and a model for the kinetic behaviour. High-pressure synchrotron X-ray diffraction demonstrates that wurtzite ZnS nanobelts have

Table 1 Comparison of the transition pressures observed in different wurtzite ZnS forms.

Wurtzite form	Transition pressure (GPa)	Reference
Bulk	0	Ref. 6
Nanocrystal	<0.5	Ref. 5
Nanobelt	6.8	This study

Figure 1 The synthesized wurtzite-structure ZnS nanobelts. a, Low-resolution SEM image; **b**, HRTEM image showing saw-like edge; **c**, electron-diffraction image; **d**, X-ray-diffraction pattern; **e**, schematic representation of the wurtzite structure; and **f**, the crystallographic dimensions of nanobelts.

a wide field of structural stability up to 6.8 GPa, remarkably different from the bulk and three-dimensional monodisperse spherical nanoparticles that transform to the sphalerite structure slowly at ambient conditions and easily with even slightly applied compression (Table 1). The transformation mechanism is explosive, not the general sluggish kinetics observed in the bulk form and nanoparticles. Theoretical calculations show that the nanobelt morphology produces a particular low-energy state that is the main reason for the improved stability of this metastable structure, in which the $\pm\{2\bar{1}0\}$ surface facets dominate the surface structure of wurtzite ZnS nanobelts. High-resolution transmission electron microscopy (HRTEM) further shows that twinning and stacking faults provide further stabilization constraints. This study not only provides an interpretation of the stability of the metastable wurtzite ZnS nanobelts, but also suggests that the controlled synthesis of stable nanobelts can be optimized to produce belts, wires or other functional units required for biological labelling or the fabrication of nano-optoelectronic devices.

Wurtzite-structure ZnS nanobelts were synthesized by a solid–vapour phase thermal-sublimation technique[11]. A scanning electron microscopy (SEM) image indicates that the as-synthesized nanobelts have a uniform cross-section along their length, with a typical width in the sub-micrometre range, extending to over 100 μm in length (Fig. 1a). HRTEM shows that partial nanobelts have a saw-like edge (Fig. 1b). X-ray and electron diffraction demonstrate that the ZnS nanobelts adopted the hexagonal wurtzite structure (Fig. 1c–e). Nanobelts are ~10 nm thick on average and have a specific growth direction along [120], with side surfaces (001) and top surfaces (010) (Fig. 1f).

The mechanical properties and structural stability of wurtzite-type ZnS nanobelts were studied in a diamond anvil cell by *in situ* high-pressure synchrotron X-ray diffraction[12]. High-pressure X-ray-diffraction patterns collected under hydrostatic (or quasi-hydrostatic at higher pressure) conditions are shown in Fig. 2. At 1 atm pressure, both X-ray-diffraction (Fig. 2) and electron-diffraction patterns (Fig. 1c) indicate that the ZnS nanobelts have hexagonal symmetry, and unit cell parameters computed from the X-ray-diffraction pattern are $a_0 = 3.7943(2)$ Å, $c_0 = 6.2679(5)$ Å and $V_0 = 78.15(8)$ Å^3, where a_0, c_0 and V_0 are the unit cell parameters calculated at ambient conditions, in agreement with the reported values of the bulk hexagonal ZnS phase[6]. Analysis of these data does not support a size-induced contraction as was observed for sphalerite with a slight tetragonal distortion from cubic symmetry[7]. Several weak X-ray-diffraction peaks occur in the observed pattern as well. As pressure approaches 6.8 GPa, several new peaks of the high-pressure phase appear, whereas the characteristic X-ray-diffraction peaks of the starting hexagonal ZnS phase drastically weaken. The newly observed peaks are consistent with the sphalerite structure. Wurtzite (w) and sphalerite (s) show a significant overlapping of w(002) and s(111), and of w(110) and s(220). On the basis of the constant intensity ratios between the three characteristic peaks of w(100), w(002) and w(101), it is obvious that the wurtzite structure remains stable to 6.8 GPa. The full-width at half-maximum (FWHM) of wurtzite peaks also does not change, so the nanobelt seems
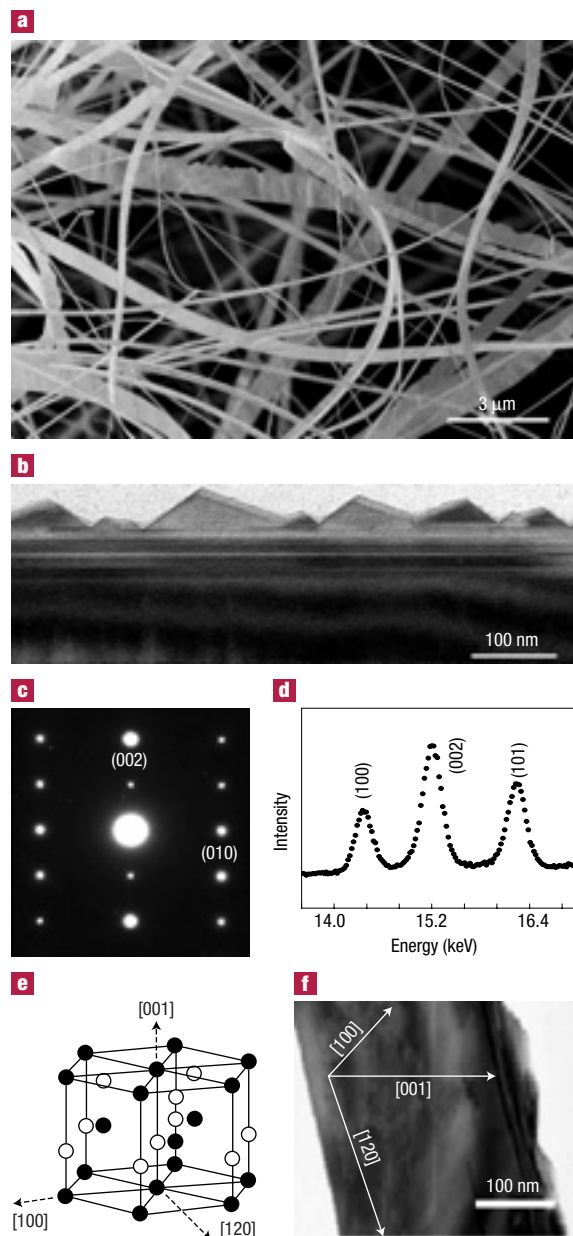
to maintain a constant shape below the transition pressure of 6.8 GPa. Above this pressure, the two peaks of w(100) and w(101) reduce significantly in intensity and become extremely weak; in contrast, the intensity of s(002) increases. Simultaneously, the new peaks show an abrupt and very noticeable broadening. These changes are interpreted as arising from a collapse of the nanobelt occurring on the wurtzite-to-sphalerite phase transformation. Such a phenomenon was previously observed in the nanowire form of the semiconductor CdSe, where the pressure-induced wurtzite-to-rocksalt phase transformation takes place[13]. Although the phase boundary was not precisely determined, it is reasonable to assume that the hexagonal phase is stable to ~6.8 GPa, and thus quickly transforms to the sphalerite structure. Organic oil pressure medium
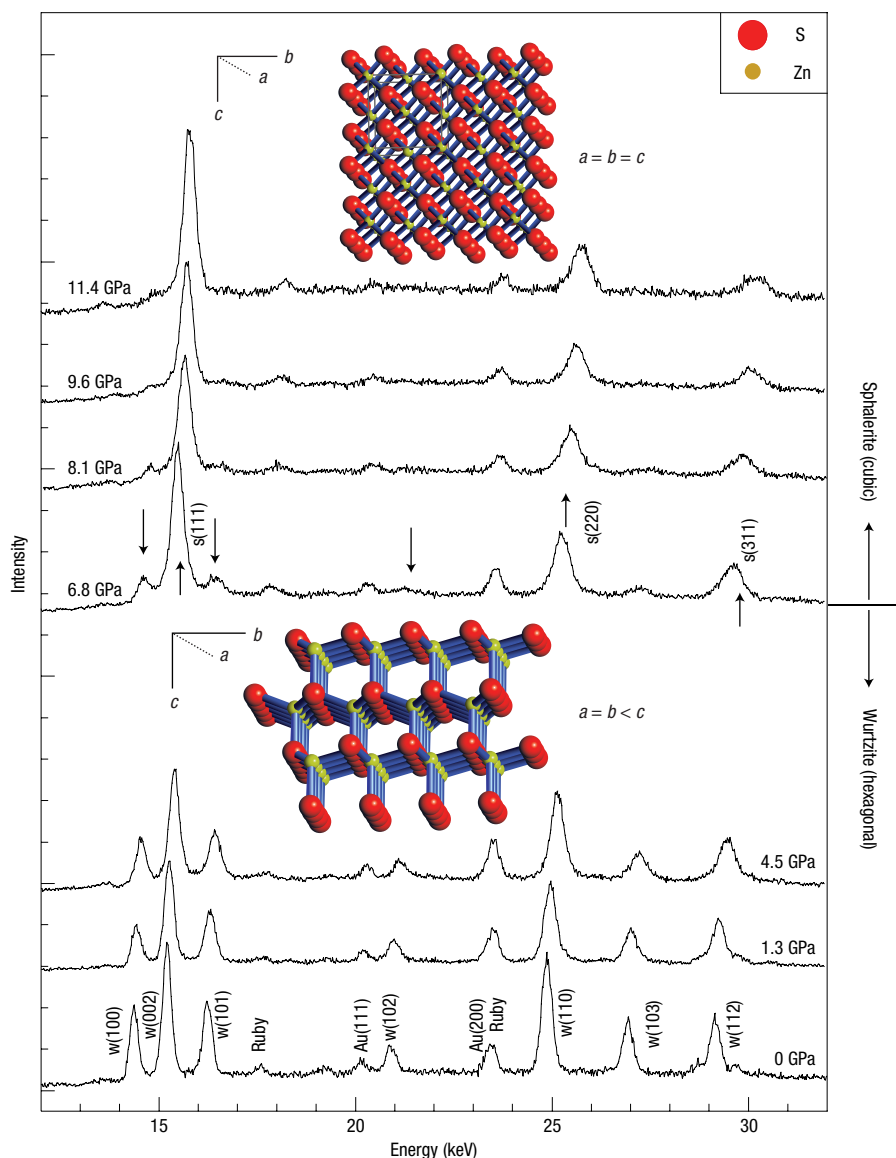
Figure 2 High-pressure X-ray-diffraction patterns of the wurtzite ZnS nanobelts. The upward and downward arrows (↑ and ↓) represent the occurrence and disappearance of X-ray-diffraction peaks of the new cubic phase and hexagonal phase. Their crystallographic characteristics are schematically shown in the two inset figures: bottom for hexagonal wurtzite and top for cubic sphalerite. Weaker X-ray-diffraction peaks are due to the small amount of gold nanoparticles used as a catalyst during synthesis and by the ruby used as a pressure calibrant.

only enables a hydrostatic state to be maintained at pressures below 5 GPa; above 5 GPa, a quasi-hydrostatic condition could generate the deviatoric stress and slight pressure gradient across the sample chamber. This may well explain the existence of a very small ratio of wurtzite phase and its extremely weak X-ray-diffraction peaks. A quick accomplishment of the phase transformation in nanobelts apparently differs from the sluggish kinetics observed in bulk and nanoparticle ZnS forms that show a wide transition-pressure range of 5–8 GPa (refs 5,7). This implies that the transformation mechanism is explosive. The resulting sphalerite phase remains stable to the peak pressure of 11.4 GPa, and is quenchable on release of pressure.

With decreasing particle size, surface energy plays a significant role in the optical and electronic properties and structural stability, in particular with extension to ambient conditions for technological applications. It is found that ZnS nanocrystals show

enhanced optical and electronic properties, but the structural stability in wurtzite does not improve in a fashion similar to bulk wurtzite[6,7]. However, because the nanocrystal is tuned to belt-like morphology, wurtzite ZnS nanobelts retain their morphology with hexagonal crystallographic symmetry to pressures as high as 6.8 GPa. It is difficult to understand this remarkable observation from simple considerations of either the thermodynamics applied in bulk materials or the nanosize-induced enhancement of surface energy[6,14,15]. We suggest that the particular morphology of the wurtzite ZnS nanobelts is responsible for the exceptional structural stability of the materials. Specifically, we show that the enhanced stability is a consequence of the fact that nanobelts are regular extended solids along the length and width of the structure, but have nanometre-scale thicknesses. A direct consequence is the very different surface-energy density on the top and bottom surfaces of a nanobelt compared with the surface-energy density

for the faces (the 'sides' of the nanobelt), which are nanometre-sized in one dimension. To explore this effect of the nanobelt morphology, we calculated the structural stability field of a wurtzite ZnS nanobelt as a function of the thickness of the nanobelt by minimizing the total free energy of the wurtzite and sphalerite taking into consideration the extra contributions associated with surface, size, morphology, shape, twinning and stacking faults, and volumetric contraction.

At 298 K and 1 atm, bulk ZnS polymorphs of wurtzite and sphalerite have a Gibbs free-energy difference of 10.25 kJ mol⁻¹, which reflects the greater stability of sphalerite compared with wurtzite[16]. With decreasing particle size, surface energy starts to play an increasingly dominant role in determining structural stability[8,14,15]. Simulations indicate that each facet associated with a well-defined diffraction plane possesses a different surface energy[17–20]. In wurtzite, (001) has the highest surface energy of $0.91-1.52$ J m⁻², whereas the (110) face has the lowest surface energy of $0.28-0.49$ J m⁻², and the (100) face has an intermediate energy of $0.52-1.0$ J m⁻². In sphalerite, both (111) and (100) faces have the two highest surface energies of 1.84 and 2.56 J m⁻², respectively, whereas the other facets have lower surface energy (<1.0 J m⁻²). The total surface energy of a three-dimensional spherical nanoparticle of wurtzite or sphalerite is then the mean surface energy, computed from the surface energy of all of the existing crystal facets that are averagely and randomly exposed on the particle surface. Accordingly, three-dimensional spherical nanoparticles of sphalerite have a mean surface energy of 0.79 J m⁻², greater than the surface energy of 0.57 J m⁻² in wurtzite[20]. The observation that the transformation temperature of sphalerite to wurtzite reduces with decreasing particle size strongly supports this surface-energy estimation[20].

The wurtzite ZnS nanobelts in this study have a specific growth direction along [120], with $\pm(2\bar{1}0)$ planes defining the two dominant surfaces (see Fig. 3 inset: top and bottom faces and Fig. 1d). Such a $\pm\{2\bar{1}0\}$-dominant surface structure is different from the common surface structure of nanocrystals that have a high percentage of cubic-, tetrahedral- and octahedral-like shapes, dominantly bounded by the combined facets of {111}, {110}, {001} and {100}; ref. 21. The surface-energy difference associated with different crystallographic planes holds a general sequence as $\gamma_{\{111\}} < \gamma_{\{100\}} = \gamma_{\{001\}} < \gamma_{\{110\}}$ in the cubic symmetry nanocrystals. The high-energy {110} surface is mostly observed in nanorods, but its instability is often observed by the formation of spherical clusters in terms of the atom sublimation, such as Au nanorods[21]. However, as a particular case, the surface energies in ZnS with hexagonal symmetry have a reverse sequence and the ($hk0$) facets, including six equal planes of $\pm(110)$, $\pm(2\bar{1}0)$ and $\pm(1\bar{2}0)$, have the lowest surface energy and so favour the formation of this type of low-energy nanobelt growing along the [120] direction with the lowest energy. As a result, the front cross-section $\pm(010)$ and side $\pm(001)$ surface faces can be neglected in the estimation of the total surface area and surface energy. A slight volumetric reduction of 1.25% takes place on the wurtzite-to-sphalerite phase transformation at 6.8 GPa. It is well known that the nucleating sphalerite crystals show predominantly the (111) plane that results directly from the (001) plane of the wurtzite phase[4]. In addition, (111) and (100) represent the two largest d-spacing planes, so both of them unambiguously dominate the surface area of the sphalerite when no specific crystal direction growth otherwise exists[21]. This is demonstrated by the observed cubic and tetrahedral morphologies of recovered nanoparticles (Fig. 3 inset: HRTEM image). Therefore, it is reasonable to assume that the newly formed sphalerite represents a structure with a higher surface energy than wurtzite. In combination with the bulk Gibbs energy ($\Delta G_{298\,K,1\,atm}$), surface-energy difference ($\Delta\gamma$) and the volumetric collapse ($P^* \Delta V$;
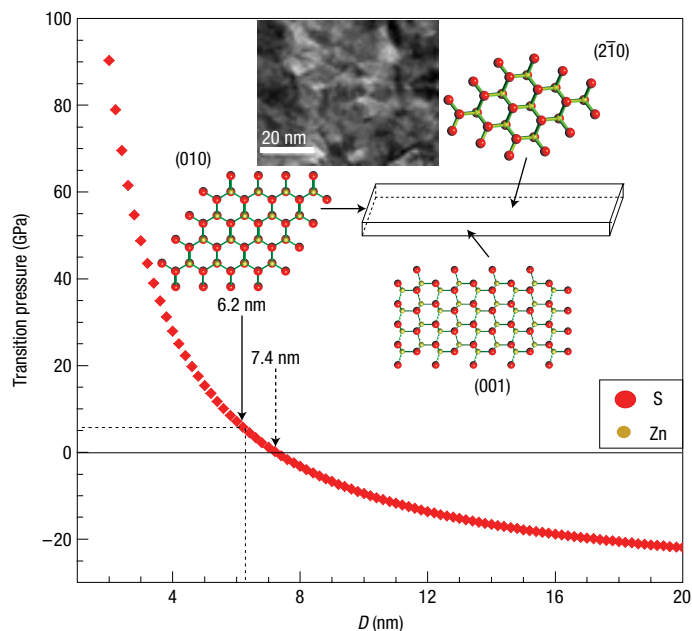

Figure 3 Correlation between the nano-thickness (**D**) and transition pressure of one-dimensional wurtzite nanobelts. Inset figures show the three characteristic surfaces and the corresponding atomic arrangements in reciprocal lattice demonstrations. Inset HRTEM figure shows that the recovered samples have the cubic and tetragonal shapes with an average size of 10 nm.

see Methods), we calculated the structural stability field of wurtzite ZnS nanobelts (the wurtzite-to-sphalerite transition pressure) as a function of nanobelt thickness. Below the critical thickness of 7.4 nm, a wurtzite nanobelt is more stable than sphalerite (Fig. 3); on reducing the thickness, the stability seems to be enhanced. In our wurtzite ZnS nanobelt, the observed transition pressure of 6.8 GPa corresponds to a calculated thickness of 6.2 nm.

Transmission electron microscopy (TEM) observation indicates that the recovered samples have an average particle size of ~10 nm (Fig. 3 inset: HRTEM image), in reasonable agreement with the particle size of ~12 nm calculated from the broad X-ray-diffraction peaks (Fig. 4). However, these values are greater than either the calculated nanobelt thickness of 6.2 nm, which corresponds to the observed transformation pressure of 6.8 GPa, or the critical thickness of 7.4 nm. Thus, a reasonable explanation may also require the incorporation of further effects induced by crystallographic defects, twins, stacking faults and volumetric contraction generated in the newly formed sphalerite on phase transformation.

Both the Zn and S atoms in wurtzite and sphalerite are four-coordinated[4,23], so the phase transformation only requires a partial atomic rearrangement. Wurtzite has the simple hexagonal-close-packed stacking order of ABABAB along the [001] direction with a resultant base of (001) and sphalerite has the cubic-close-packed stacking order of ABCABC along the [111] direction with the characteristic crystallographic facet of (111); ref. 23. On transformation from wurtzite to sphalerite, the (001) plane of wurtzite converts directly to the (111) plane of sphalerite[22,24]. On the basis of such a fundamental genetic relation and combined with the particular crystallographic characteristics of the two ZnS polymorphs, two types of transformation mechanism can be suggested (Fig. 5). The first involves the rearrangement of three {ZnS} layers (Fig. 5a), leading to (111) twinning in sphalerite

Figure 4 Comparison of the three characteristic X-ray-diffraction peaks between wurtzite and sphalerite polymorphs at 1 atm pressure. Here w and s represent the wurtzite and sphalerite, respectively.

related by a 180° rotation (Fig. 5b). The second involves the rearrangement of four {ZnS} layers (Fig. 5c), resulting in the development of stacking faults (Fig. 5d). It seems that the transformation initiated by the first type of atomic rearrangement requires a higher energy than the second type of transition mechanism, because the rotation in the first type of mechanism is produced as a consequence of a faulted stacking of perfect crystals, and the bonding configuration at the stacking faults and the twin boundaries remains close to that of the perfect structure[24].

The two types of mechanism have been observed in the HRTEM images taken from the recovered sphalerite (Fig. 5e,f) that show the formation of the boundary twins (ABCACBA) (Fig. 5e) and stacking faults (for example, the double stacking faults shown in Fig. 5f). From a thermodynamic viewpoint, the resultant stacking faults and twins imply a high-energy sphalerite structure. Although numerous types of energy contribution, as suggested above, are added to the total energy of sphalerite, the nanobelt thickness (also including the critical thickness) could be significantly greater for the wurtzite nanobelts that transform to sphalerite at modelled pressure with thinner thickness. It has been observed that sphalerite nanoparticles show a size-induced contraction by undergoing a tetragonal distortion from the cubic structure, which leads to a volumetric decrease of the order of ~2% compared with bulk sphalerite with cubic symmetry[7]. At the transition pressure of 6.8 GPa, this could result in an energy change as large as ~12.5 kJ mol^{-1} between sphalerite and wurtzite, responsible for a transition pressure jump of ~2.4 GPa. Combining the contributions from the above-mentioned factors provides an understanding of the high transition pressure of 6.8 GPa in the wurtzite ZnS nanobelts synthesized here.

In summary, we have observed an enhanced stability field and the explosive phase-transformation mechanism for wurtzite ZnS nanobelts that are understood by concentrating on the particular morphology and shape using the combined techniques of *in situ* high-pressure synchrotron X-ray-diffraction measurements, theoretical calculations and HRTEM investigation. The enhanced stability field shows that the specific morphology of wurtzite ZnS nanobelts represents the most-favourable low-energy surface structure, which has a dominant effect in controlling the formation and structural stability of nanobelts. Owing to the similarities between semiconductors, application of this mechanism to the creation of further metastable phases could open up the possibility for manipulating the surface energetics of different semiconductor

Figure 5 Schematic representation of the wurtzite-to-sphalerite phase transformation. **a,b**, The first (1) involves the rearrangement of three {ZnS} layers (**a**), leading to (111) twinning in sphalerite related by a 180° rotation (**b**). **c,d**, The second (2) involves the rearrangement of four {ZnS} layers (**c**), resulting in the development of stacking faults (**d**). **e–g**, Filtered HRTEM images of the samples: starting wurtzite phase (**e**); recovered sphalerite phase (**f,g**).

nanoforms in a controlled manner that could have practical consequences[8,9,25,26]. Accordingly, the synthesis of stable and reliable nanobelts, quantum wells or wires with specific sizes and thickness (<10 nm) can be obtained by adjusting the surface energy, morphology and intrinsic structure with near-atomic precision that may prove to be applicable in electronics, optics and sensors.

METHODS

pressures of ~11.4 GPa were used for structure analysis and cell-parameter refinement. The recovered samples were also examined by SEM and TEM.

Particle sizes are estimated by TEM and the FWHM of the observed X-ray-diffraction peaks. The standard Scherrer's equation for energy dispersive X-ray diffraction is modified as

$$\tau = (0.94 \times Ed)/\Delta E,$$

where τ is the particle size in ångströms, E and ΔE are the energy and FWHM of the observed Bragg peak in keV and d is the inter-planar spacing in ångströms.

Theoretical calculations are based on the total Gibbs energy difference between the two ZnS polymorphs of wurtzite and sphalerite in combination with the size-induced surface-energy contribution. At 1 atm, the Gibbs thermodynamic equation is modified as $\Delta G = \Delta H - T\Delta S + \Delta \gamma s$, where ΔG, ΔH, ΔS and $\Delta \gamma$ represent the difference of the Gibbs free energy, enthalpy, entropy and the unit surface energy between wurtzite and sphalerite, respectively, and s is the surface area. To evaluate the reliability for the simulated surface energies of the surface planes[17–20] used in this study, the temperature at $\Delta G = 0$ for each particle size is calculated, in agreement with the synthesized temperatures[10,20]. In wurtzite ZnS nanobelts, the surface energy is dominated by the $\pm(2\bar{1}0)$ facets, and in the newly formed sphalerite nanocrystals, it is dominated by (111) and (100) facets. The corresponding cubic and tetragonal morphologies are characterized in the recovered samples (Fig. 3 inset: HRTEM image). At a certain thickness of nanobelt, the Gibbs free-energy difference ($\Delta G_{298\,K}^{1\,atm}$) at 298 K and 1 atm pressure can be calculated. On compression, although the energy gap of $\Delta G_{298\,K}^{1\,atm}$ is overcome by a newly added energy term of $P^* \Delta V$, wurtzite theoretically transforms to the sphalerite phase. Here, P^* and ΔV represent the transition pressure of the wurtzite-to-sphalerite phase transformation and the volumetric difference between the two ZnS polymorphs at P^*, respectively.

References

1. Monroy, E., Omnes, F. & Calle, F. Wide-band gap semiconductor ultraviolet photodetectors. *Semicond. Sci. Technol.* **18,** R33–R51 (2003).
2. Bhargava, R. N., Gallagher, D., Hong, X. & Nurmikko, D. Optical properties of manganese-doped nanocrystals of ZnS. *Phys. Rev. Lett.* **72,** 416–419 (1994).
3. Park, W., King, J. S., Neff, C. W., Liddell, C. & Summers, C. ZnS-based photonic crystals. *Phys. Status Solidi b* **229,** 949–960 (2002).
4. Gilbert, B. *et al.* X-ray absorption spectroscopy of the cubic and hexagonal polytypes of zinc sulfide. *Phys. Rev. B* **66,** 245205 (2002).
5. Qadri, S. B. *et al.* The effect of particle size on the structural transitions in zinc sulfide. *J. Appl. Phys.* **89,** 115–119 (2001).
6. Desgreniers, S., Beaulieu, L. & Lepage, I. Pressure induced structural changes in ZnS. *Phys. Rev. B* **61,** 8726–8733 (2000).
7. Qadri, S. B. *et al.* Size-induced transition-temperature reduction in nanoparticles of ZnS. *Phys. Rev. B* **60,** 9191–9193 (1999).
8. Alivisatos, A. P. Semiconductor clusters, nanocrystals, and quantum dots. *Science* **271,** 933–937 (1996).
9. Lieber, C. M. One-dimensional nanostructures: chemistry, physics applications. *Solid State Commun.* **107,** 607–616 (1998).
10. Zhao, Y. W. *et al.* Low-temperature synthesis of hexagonal (wurtzite) ZnS nanocrystals. *J. Am. Chem. Soc.* **126,** 6874–6875 (2004).
11. Ma, C., Moore, D., Li, J. & Wang, Z. L. Nanobelts, nanocombs, and nanowindmills of wurtzite ZnS. *Adv. Mater.* **15,** 228–231 (2003).
12. Wang, Z. W. *et al.* A quenchable superhard carbon phase synthesized by cold compression of carbon nanotubes. *Proc. Natl Acad. Sci. USA* **101,** 13699–13702 (2004).
13. Zaziski, D. *et al.* Critical size for fracture during solid-solid phase transformations. *Nano Lett.* **4,** 943–946 (2004).
14. Chen, C. C., Herhold, A. B., Johnson, C. S. & Alivisatos, A. P. Size dependence of structural metastability in semiconductor nanocrystals. *Science* **276,** 398–401 (1997).
15. Tolbert, S. H. & Alivisatos, A. P. The wurtzite to rock salt structural transformation in CdSe nanocrystals under high pressure. *J. Chem. Phys.* **102,** 4642–4656 (1995).
16. Barin, I., Knacke, O. & Kubschewski, O. *Thermochemical Properties of Inorganic Substances* 827–828 (Springer, Berlin, 1977).
17. Hamad, S., Cristol, S. & Catlow, C. R. Surface structures and crystal morphology of ZnS: Computational study. *J. Phys. Chem. B* **106,** 11002–11008 (2002).
18. Wright, K., Watson, G. W., Parker, S. C. & Vaughan, D. J. Simulation of the structure and stability of sphalerite (ZnS) surfaces. *Am. Mineral.* **83,** 141–146 (1998).
19. Wright, K. & Gale, J. D. Interatomic potentials for the simulation of the zinc-blende and wurtzite forms of ZnS and CdS: Bulk structure, properties, and phase stability. *Phys. Rev. B* **70,** 035211 (2004).
20. Zhang, H. Z., Huang, F., Gilbert, B. & Banfield, J. F. Molecular dynamics simulations, thermodynamic analysis, and experimental study of phase stability of zinc sulfide nanoparticles. *J. Phys. Chem. B* **107,** 13051–13060 (2003).
21. Wang, Z. L. Transmission electron microscopy of shape-controlled nanocrystals and their assemblies. *J. Phys. Chem. B* **104,** 1153–1175 (2000).
22. Williams, V. A. Diffusion of some impurities in zinc sulfide single crystals. *J. Mater. Sci.* **7,** 807–812 (1972).
23. Birman, J. L. Simplified LCAO method for zincblende, wurtzite, and mixed crystal structures. *Phys. Rev.* **115,** 1493–1905 (1959).
24. Posfai, M. & Buseck, P. R. in *Modular Aspects of Minerals* Vol. 1 (ed. Merlino, S.) 193–235 (EMU Notes in Mineralogy, Eötvös Univ. Press, Budapest, 1997).
25. Alivisatos, P. The use of nanocrystals in biological detection. *Nature Biotechnol.* **22,** 47–52 (2004).
26. Ding, Y., Wang, X. D. & Wang, Z. L. Phase controlled synthesis of ZnS nanobelts: zinc blende vs wurtzite. *Chem. Phys. Lett.* **398,** 32–36 (2004).

Competing financial interests

The authors declare that they have no competing financial interests.

Reprints and permission information is available online at http://npg.nature.com/reprintsandpermissions/